Structure of a two-dimensional epitaxial Er silicide on Si(111) investigated by Auger-electron diffraction

P. Wetzel, C. Pirri, P. Paki, D. Bolmont, and G. Gewinner
Laboratoire de Physique et de Spectroscopie Electronique, Faculté des Sciences et Techniques, 4 rue des Frères Lumière 68093, Mulhouse CEDEX, France

(Received 23 June 1992; revised manuscript received 14 October 1992)

Annealing at 400 °C of one Er monolayer deposited on Si(111) results in a $p(1\times1)$ two-dimensional epitaxial silicide with a remarkable degree of perfection. In the present study, Auger and photoelectron diffraction is used to investigate the atomic structure of this surface silicide. The Er *MNN* Auger-intensity polar profiles as well as the photoemission intensities of the characteristic surface bands measured along the opposite $[\bar{1}2\bar{1}]$ and $[1\bar{2}1]$ azimuths display a typical asymmetry that implies the formation of one domain of a silicide with $p3m1$ symmetry. A comparison of the Er *MNN* polar profiles with single-scattering cluster simulations demonstrates that the hexagonal Er monolayer is accommodated underneath a buckled Si layer similar to a Si(111) double layer in the substrate. The buckling is found to be comparable to Si(111) (0.90 Å, as opposed to 0.78 Å in Si) and the Er-Si interlayer spacing is contracted with respect to bulk $ErSi_{1.7}$ (1.80 Å, as opposed to 2.045 Å).

I. INTRODUCTION

The physical and chemical properties of ultrathin films are of considerable interest for both scientific and technological reasons. The reduced coordination and symmetry in such layers lead to important changes in crystallographic and electronic structure with respect to the same material in bulk form. This offers the opportunity to study new and exotic phenomena and so holds out the promise of new device applications. In particular, two-dimensional (2D) overlayers on solid surfaces constitute a suitable class of systems for studying fundamental aspects of ordering. They are also attractive to model by computer-simulation techniques. A key question and goal is the preparation of two-dimensional layers in a controlled way.

Because of their favorable properties in view of applications in the microelectronic industry the rare-earth silicides have been thoroughly investigated in the past few years. In particular, the erbium disilicide is of special interest since it can be grown epitaxially on monocrystalline Si.[1–4] Moreover, this silicide is characterized by a very low Schottky barrier to *n*-type Si[5] combined with a small electrical resistivity[6] and is therefore attractive for the Si based technology.

The hexagonal Er silicide crystallizes in the AlB_2-type structure. Along the [0001] direction the $ErSi_2$ structure consists of a stack of alternating hexagonal Er planes and graphitelike Si planes. Experimentally the perfect $ErSi_2$ structure is not observed in epitaxial growth on Si(111). A nonstoichiometric form $ErSi_{1.7}$ which contains an ordered array of Si vacancies is observed instead, giving rise to a $\sqrt{3}\times\sqrt{3}\ R30°$ superstructure in the (0001) plane. Bulklike (≥ 10 monolayers) Er silicide films exhibit a reconstructed (0001) surface termination probably made of a buckled Si double layer.[7] We have undertaken a detailed study of epitaxial Er silicide films versus thickness. In particular, important information on these highly ordered systems can be obtained by studying the earliest submonolayer film growth stages.

In a recent paper,[7] we demonstrate that upon Er deposition and subsequent annealing at 400 °C, layer by layer growth takes place up to one monolayer (ML) and an epitaxial two-dimensional Er silicide with a very high degree of structural perfection is formed. This silicide turns out to be highly attractive from a fundamental point of view since it exhibits remarkably sharp and strongly dispersive surface bands.[8] The 2D Fermi contour has been determined and consists of a tiny hole pocket around the $\bar{\Gamma}$ point, and a tiny electron pocket around the $\bar{M}$ point of the surface Brillouin zone (SBZ). This is characteristic of a semimetal with a rather small density of states at the Fermi level. It is well known that the Fermi surface structure has many implications on a large variety of macroscopic and microscopic phenomena.[9] Moreover, an interesting and technologically important property of the surface silicide is its extremely low reactivity with respect to residual gases of the UHV system. Hence this silicide possibly provides a good starting point for obtaining highly ordered heterostructures.

To our best knowledge, this is the first observation of epitaxial growth of a well-ordered 2D silicide. The latter can be readily distinguished from its three-dimensional counterpart by low-energy electron diffraction (LEED). LEED shows a $p(1\times1)$ as opposed to the $\sqrt{3}\times\sqrt{3}\ R30°$ pattern observed on thick epitaxial $ErSi_{1.7}$ layers. Preliminary x-ray photoelectron diffraction data suggest that the atomic structure of this surface compound can be viewed as a single epitaxial $ErSi_2$ layer without Si vacancies but with a reconstructed Si top layer.[7] It was concluded that this reconstruction may be similar to the one observed at the (0001) surface of thick epitaxial $ErSi_{1.7}$ (or related $YSi_{1.7}$) films.

The goal of the present study is to gain more insight

into the structure of this 2D silicide. Structural information is inferred from elastic scattering of Auger and photoelectrons originating in the silicide layer. It is now well established that in favorable cases the dominant forward-scattering processes at relatively high kinetic energies (≥ 500 eV) provide a rather direct identification of the emitter-scatterer bond directions for those scatterers lying above the emitter.[10,11] Er *MNN* Auger peak intensity polar profiles show prominent forward-scattering enhancements which indeed allow us to roughly locate the Si atoms in the reconstructed top layer by simple real-space triangulation. In this respect, the data indicate that the hexagonal Er monolayer is accommodated underneath a buckled Si double layer which adopts a geometry similar to a Si(111) double layer in bulk Si. However, it appears that reasonably accurate structural determination is only obtained by single-scattering cluster modeling. In the present favorable case single scattering provides a remarkably good description of the Auger intensity profiles. The calculations show the best fit to experiment for a buckling of 0.90 Å, somewhat larger than in Si(111), and an Er-Si interlayer spacing of 1.80 Å, i.e., a contraction of $\sim 10\%$ with respect to bulk $ErSi_{1.7}$.

The surface silicide has the same $p3m1$ symmetry as the ideal Si(111) surface and only a single domain is actually formed. The relevant threefold rotational symmetry is also reflected in a striking asymmetry of the photoemission intensities from 2D band features observed at equivalent $k_{\parallel}$ points along the $\bar{\Gamma}\bar{M}$ lines of the SBZ corresponding to opposite $[\bar{1}2\bar{1}]$ and $[1\bar{2}1]$ azimuths. In the geometry used in our experiments this asymmetry must originate in the silicide structure itself. This confirms that the $(1\bar{2}1)$ plane is not a mirror plane for the surface silicide. In contrast, the relevant 2D energy-band dispersions $E(k_{\parallel})$ are quite symmetric with respect to this plane as expected from time-reversal symmetry which ensures that $E(k_{\parallel})=E(-k_{\parallel})$.

II. EXPERIMENT

The experiments were performed in standard UHV interconnected preparation and analysis chambers (base pressure 1.10^{-10} mbar). The hemispherical energy analyzer was set to a 2° full acceptance angle. Unpolarized He_I and high power x-ray source Al $K\alpha$ photons at 21.2 eV and 1486.6 eV, respectively, were used as excitation for valence band and core-level (Auger) photoelectrons (electrons), respectively. In our spectrometer angle resolved data are collected by rotating the Si(111) substrate, the angle between incident light and electron analysis being kept constant. The experimental geometry and its relation to the SBZ is shown in Fig. 1. The measured energy and polar angle of emission Θ (referred to the surface normal) of the photoelectron determine $\mathbf{k}_{\parallel}$, its wave-vector component in the surface plane. There are three equivalent $[\bar{1}2\bar{1}]([1\bar{2}1])$ azimuths corresponding to $\mathbf{k}_{\parallel}$ points along the $\bar{\Gamma}\bar{M}(\bar{\Gamma}\bar{M}')$ symmetry lines and six equivalent $[10\bar{1}]$ azimuths corresponding to the $\bar{\Gamma}\bar{K}$ symmetry line if one considers the symmetry group of the Si(111) substrate or ideal surface.

Clean surfaces of Si(111) were prepared by cycles of

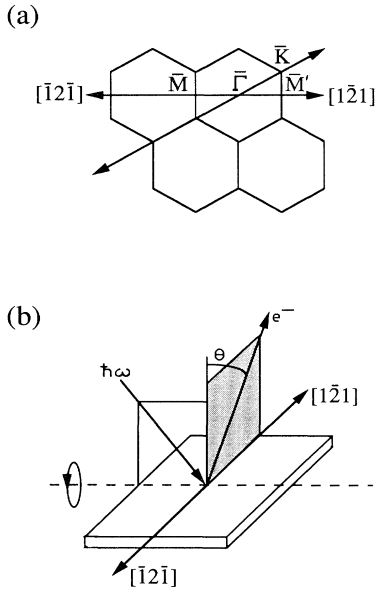

FIG. 1. (a) The (1×1) surface Brillouin zone with the main directions of analysis and (b) the experimental geometry.

Ar^+ ion sputtering and annealing at 800 °C. Very sharp (7×7) LEED patterns were observed after annealing. The erbium was then evaporated from a boron nitride crucible heated by an electron beam. The Er film thickness was monitored by using a carefully calibrated quartz-crystal balance. The deposition rates were chosen to be ~ 1 ML/mn. 1 ML corresponds to a single Si(111) atomic layer density, i.e., 7.83×10^{14} cm^{-2}. Deposition of 1 ML Er at room temperature results in a disordered phase as evidenced by a weak diffuse (1×1) LEED pattern and the absence of structure in the angular distribution of core-level photoemission intensities.[7] Yet upon annealing at 400 °C for 10 mn the (1×1) diffraction pattern becomes very sharp and displays a remarkable threefold symmetry even at the lowest electron energies (~ 20 eV). At this stage, prominent energy bands with a nearly perfect 2D character attest to the formation of a well-ordered surface compound.[8]

III. SINGLE SCATTERING MODELING

The single-scattering simulations used in the present study are based on the simple model first used by Kono *et al.*[12] to interpret their O(1*s*) photoelectron diffraction data from Cu(001) $c(2\times2)$-O. In the present case of Auger-electron emission no polarization effects are included and the primary wave excited from a given Er site is approximated by an *s* wave. Purely atomic plane-wave scattering amplitudes are utilized but a correction has been made for the spherical wave effects.[13] This results in a percentage of intensity modulations which compares more favorably with experiment. However the same structural conclusions are arrived at when no correction is made. We have taken the following parameters in the calculations for Er *MNN* emission: electron kinetic ener-

gy, 1430 eV; isotropic electron mean free path, 15 Å; isotropic mean squared vibration amplitude, 0.015 Å^2; and inner potential $V_0 = -12$ eV. As expected from the strong forward-scattered amplitude, test calculations show that at low polar angles only the scattering by the nearest Si neighbors located just above the Er layer is significant. However, at higher polar angles ($\Theta \geq 50°$, grazing emission) a much larger cluster size is needed in order to simulate the experimental data. We have adopted a cluster containing ~100 Er and ~200 Si atoms in all calculations presented. At the polar angles studied in this work ($\Theta \leq 80°$) only Si atoms located above the Er monolayer significantly contribute to the scattering of the Er emission.

IV. RESULTS AND DISCUSSION

Figure 2 shows the experimental polar profiles of the Auger Er *MNN* intensity along the three different azimuthal orientations of the crystal, namely $\bar{\Gamma}\bar{M}$, $\bar{\Gamma}\bar{M}'$, and $\bar{\Gamma}\bar{K}$ corresponding to $[\bar{1}2\bar{1}]$, $[1\bar{2}1]$, and $[10\bar{1}]$ crystallographic directions, respectively. The Er *MNN* Auger transition was chosen because it does not interfere with photoemission from Si emission in contrast with the strong Er 4*f* core levels which partly overlap the broad Si 3*s* valence-band feature. This ensures the absence of any modulations from Si emission and thus the strict element specificity of the technique. Any structure in these curves must reflect the atomic environment of the Er species. Since the kinetic energy of the Er *MNN* Auger electrons is 1430 eV, forward scattering along the nearest-neighbor bond directions is expected to dominate the intensity modulations. As can be seen, a completely featureless polar profile is observed along $\bar{\Gamma}\bar{K}$, i.e., the six azimuths equivalent to $[10\bar{1}]$. This profile closely corresponds to the instrumental response function measured on the disordered phase obtained by Er deposition at room temperature. The lack of any significant structure along $\bar{\Gamma}\bar{K}$ implies the absence of Si (or Er) scatterers above the Er in the $(1\bar{2}1)$ (or equivalent) crystallographic planes.

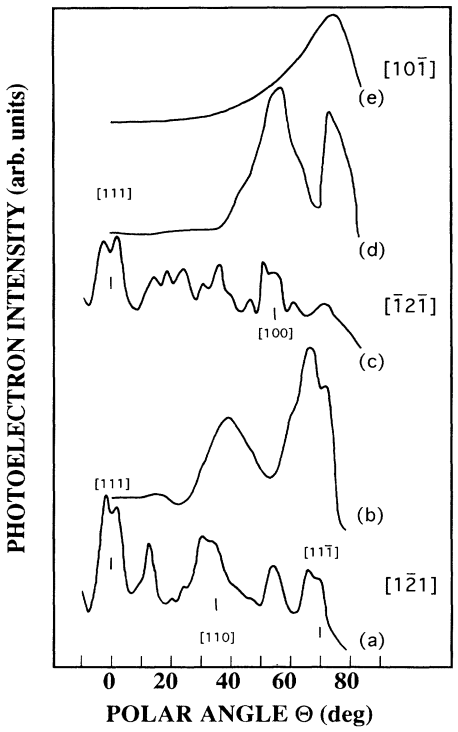

FIG. 2. Polar-angle scans of Er *MNN* Auger emission for the Er surface silicide along the (b) $[1\bar{2}1]$, (d) $[\bar{1}2\bar{1}]$, and (e) $[10\bar{1}]$ crystallographic directions. Also shown are the Si 2*p* core-level intensity profiles from a clean Si(111) substrate recorded along the two opposite (a) $[1\bar{2}1]$ and (c) $[\bar{1}2\bar{1}]$ azimuths. Important crystallographic directions and angles associated with simple forward-scattering events expected for the Si monocrystal are indicated for the Si 2*p* profiles.

Consider now the data obtained along the $\bar{\Gamma}\bar{M}$ and $\bar{\Gamma}\bar{M}'$ azimuths it is apparent that the profiles are quite different along the opposite $[\bar{1}2\bar{1}]$ and $[1\bar{2}1]$ directions and now show prominent intensity enhancements at specific polar angles. Measurements along equivalent azimuths of the Si(111) substrate give identical results within experimental uncertainty thus confirming the asymmetric distribution. Obviously the surface silicide structure exhibits exactly the same threefold rotational symmetry as the substrate with only one kind of mirror planes namely $(10\bar{1})$ and equivalent planes. This is consistent with the LEED observations in normal incidence which clearly reflect the threefold rotation axis even at very low energies where the electrons mainly probe the surface structure. The $p3m1$ symmetry of the surface silicide can be opposed to the sixfold rotational symmetry of the ideal AlB_2 structure of $ErSi_2$. Yet it is the expected symmetry if the surface silicide adopts a structural model like that depicted in Fig. 3. This atomic arrangement can be derived in a simple way from a single $ErSi_2$ layer (AlB_2 structure) by moving upwards every second Si atom in the top Si(0001) plane. Such a buckling at the surface is expected on physical grounds because of the compression present in the graphitic Si(0001) plane which leads to the formation of Si vacancies in bulk $ErSi_{1.7}$. The nearest-neighbor Si-Si interatomic distance is 2.18 Å in $ErSi_{1.7}$ as opposed to 2.35 Å in Si.

Now, we show that simple inspection of the Er *MNN* intensity profiles supports the model depicted in Fig. 3 as far as the Si top layer geometry is concerned and allows us to roughly locate this layer with respect to the Er monolayer. First, let us note that one observes a clear-cut threefold rotational symmetry and the absence of scatterers in the $(1\bar{2}1)$ plane. This implies that the Si species must be located on top of the threefold hollows of the hexagonal Er monolayer. A different kind of reconstruction, for instance, the alternative location on top of the Er atoms is incompatible with the absence of scatterers in the $(1\bar{2}1)$ planes. This requirement implies that the only possible structural change in the surface silicide with respect to its 3D $ErSi_2$ counterpart is a buckling of the Si top layer by moving upwards one of the two Si atoms per surface cell, i.e., by allowing them to become inequivalent. The structure observed in the Auger-intensity

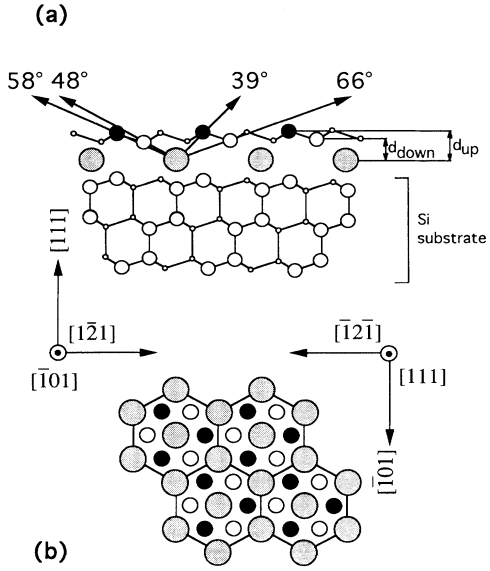

FIG. 3. (a) A sketch of the atomic structure of the Er surface silicide projected along the [$\bar{1}$01] direction and (b) a top view of the same structure. Large solid circles refer to the Er atoms and small solid circles to the Si top layer atoms. In (a) the large and small open circles represent Si atoms in the plane of the paper, and in the ($\bar{1}$01) plane immediately above the paper, respectively. Also indicated are the forward-scattering angles expected in the polar profiles of Er *MNN*. The interfacial geometry adopted is tentative and corresponds to the T_4 registry discussed in the text.

profiles along inequivalent [$\bar{1}$2$\bar{1}$] and [1$\bar{2}$1] azimuths can indeed be understood in terms of scattering at two inequivalent Si atoms in the top layer. Along [1$\bar{2}$1] one observes two strong structures at 39° and about 66° polar angles that may be assigned to forward scattering at Si_{up} and Si_{down} atoms, respectively, as depicted in Fig. 3. The peak at 39° is very similar to the one attributed to forward scattering at the similarly reconstructed $YSi_{1.7}$ surface.[14] It's full angular width at half maximum of ~14° seems consistent with the expected width of forward scattering at a single Si atom in the top layer. The present situation is comparable to the one encountered in photoelectron diffraction in adsorbed molecules, for instance, C(1*s*) emission scattered by O in chemisorbed CO.[15] Actually the 66° and (to a much lesser extent) the 39° features show some distinct fine structure which obviously complicates the interpretation in terms of forward-scattering peaks. Nevertheless, let us assume at this stage that the angular positions of the centroids of the 39° and 66° features gives us the Er-Si bond directions. Hence simple triangulation yields a distance of ~2.7 Å for Si_{up} and ~2.0 Å for Si_{down} atoms above the Er plane. This is comparable to the values observed at the reconstructed $YSi_{1.7}$ surface.[14] The observed buckling suggests a geometry of the Si top layer essentially similar to a Si(111) double layer in bulk Si. Moreover the Er-Si_{down} interplane distance of about 2.0 Å is very close to the value of 2.045 Å measured in bulk $ErSi_{1.7}$.

As shown in Fig. 3 within the above geometry deduced from the data along [1$\bar{2}$1] the Er-Si bond directions are expected to yield forward-scattering features at 48°, 58°, and 77° in polar intensity profiles taken along the opposite [$\bar{1}$2$\bar{1}$] azimuth. The experiment shows a peak centered about 75° and a broad more complex feature centered at 55° with shoulders on both sides. The 75° feature is close to the expected direction. On the other hand the complex structure near 55° is indeed located near the expected forward-scattering directions at 48° and 58°. However, it is clear that the observed structure is not merely the superposition of two peaks at 48° and 58°. Possibly, this results from the fact that the 48° and 58° directions are so close that amplitudes of forward scattering at both Si_{up} and Si_{down} atoms are strong in the directions lying in between where they interfere constructively and give rise to a strong enhancement near 55°. Thus the Auger-electron diffraction data observed along [$\bar{1}$2$\bar{1}$] seem to be roughly consistent with the location of the atoms in the Si top layer inferred from the data along [1$\bar{2}$1].

Although valuable information is obtained from the above discussion, it is apparent that at this level of interpretation a reasonably accurate structural determination cannot be achieved. Even in the present rather simple system, except the peak at 39°, most structures exhibit quite complex shapes. Hence the concept of peak position has no obvious meaning and, in turn, an accurate bond direction cannot be determined. Moreover, there is no reliable means to distinguish between zeroth-order forward-scattering peaks and first-order interference features.

In an attempt to obtain more detailed structural information we now compare the experimental data, corrected for the instrumental response, to single-scattering simulations. There are only two structural parameters of relevance here in the model of Fig. 3, namely the distances d_{up} and d_{down} of the Si_{up} and Si_{down} atoms, respectively, to the underlying Er atomic plane. As expected our test calculations show that for $\Theta \leq 80°$ the profiles are not sensitive to the atomic geometry below the Er monolayer, such as, for instance, the distance to the Si substrate. Figure 4 compares the experiment along [1$\bar{2}$1] to simulations for different values of d_{up} with $d_{down} = 1.80$ Å kept constant. First, we note a good overall agreement in shape of all structures. The fine structure is rather well reproduced in particular for the feature near 66°. The peak at 39° is essentially a pure forward-scattering peak which originates in scattering at the Si_{up} atom in agreement with the above qualitative discussion. Calculations (not shown) indicate that the related first-order interference feature near 18° as well as the peak position are already correctly predicted when the cluster includes only the Er emitter and the nearest Si_{up} atom. As can be seen in Fig. 4, its angular position directly follows the change in d_{up}. The best agreement is obtained for $d_{up} = 2.70 \pm 0.10$ Å. The angular width of this peak is ~14° significantly larger than predicted. Possible origins of this difference include the approximate scattering factors, enhanced anisotropic thermal vibrations, structural disorder, and angular averaging. On the other hand, the

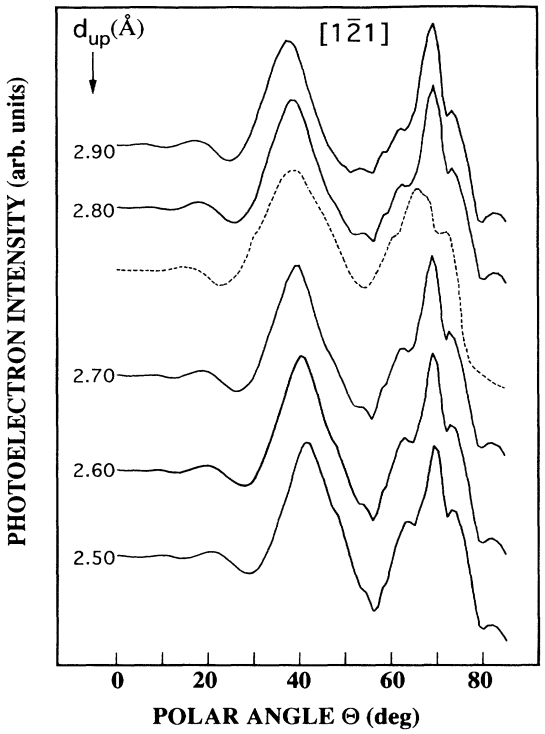

FIG. 4. Comparison of the experimental Auger *MNN* polar profiles along the [1$\bar{2}$1] azimuth (dotted line) to single-scattering cluster simulations (solid lines) for various d_{up} and $d_{down}=1.80$ Å kept constant. The experimental data are corrected for the instrumental response function in order to make them directly comparable to the calculations.

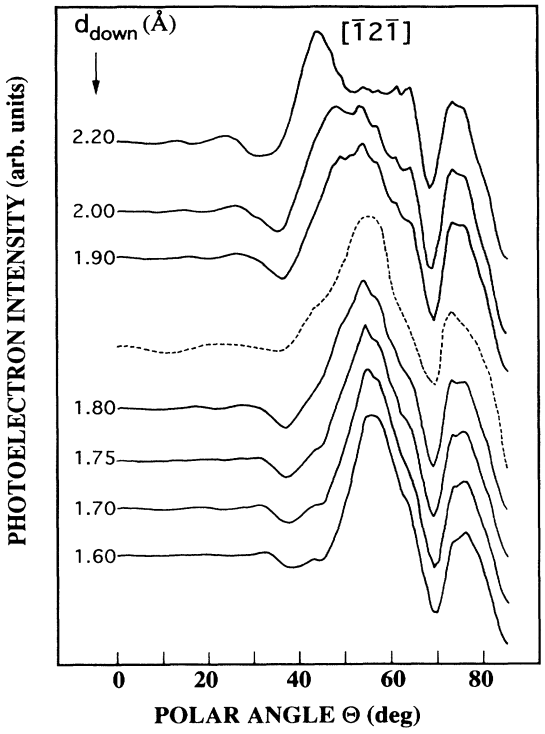

FIG. 5. Same as a Fig. 4 but along [$\bar{1}$2$\bar{1}$] and for various d_{down} with $d_{up}=2.70$ Å kept constant.

complex structure near 66° displays less sensitivity to d_{up}. This seems again consistent with our qualitative discussion which attributes this feature mainly to scattering at Si_{down} atoms. However, the calculations demonstrate that at these larger polar angles up to ~200 Si atoms including both Si_{up} and Si_{down} atoms must be included in the (spherical) cluster in order to reproduce the experimental shape.

Figure 5 now compares the experiment along [$\bar{1}$2$\bar{1}$] to single-scattering calculations for different values of d_{down} with $d_{up}=2.70$ Å kept constant at its optimal value. It is apparent that the complex structure near 55° displays a great sensitivity to d_{down} and the best fit is observed for $d_{down}=1.80\pm0.10$ Å. The shape and location of all structures in the experiment are then remarkably well reproduced. It is clear that the agreement is not satisfactory for the value of $d_{down}=2.0$ Å inferred from qualitative reasoning in terms of forward-scattering peaks along the [1$\bar{2}$1] azimuth. On the other hand, the peak near 75° remains nearly unaffected by changes in the d_{down} parameter. Again scattering at a large number of Si_{up} and Si_{down} atoms contributes to this feature.

Overall the simulations based on single scattering provide a remarkably good description of the data. This is not too surprising since multiple scattering is only expected to become important at large polar angles (grazing emission) where rows of scatterers may be encountered in the forward-scattering cones from nearest neighbors. The values of $d_{up}=2.70$ Å and $d_{down}=1.80$ Å obtained in the present study indicate a buckling (0.90 Å) of the Si layer slightly larger than in bulk Si(111). On the other hand, the Er-Si_{down} interlayer spacing (1.80 Å) contracts by ~10% with respect to the Er-Si interlayer distance in bulk $ErSi_{1.7}$ (2.045 Å).

The physical origin of this contraction probably lies in the enhanced Er-Si_{down} (weakened Er-Si_{up}) bond strengths for the buckled Si layer, as compared to the flat graphite-like Si(0001) plane where all Si-Er interactions are equivalent. Thus the Er-Si interplane distance in bulk $ErSi_{1.7}$ is expected to lie between the Er-Si_{down} and Er-Si_{up} interplane distances. The presence of the surface may also favor a stronger binding of Si top double layer to the Er. On the other hand the buckling is larger than in bulk Si. This is consistent with a charge transfer from Er to the Si top layer since a larger buckling implies an evolution of the dangling bond from sp_3 to more *s*-like orbital character. This, in turn, is accompanied by a lowering of the dangling-bond energy and a filling of the dangling-bond band observed in photoemission.[8]

An important point is that only one domain of surface silicide with 3-m point-group symmetry is actually formed. If this were not the case one should observe a peak at 39° in the [$\bar{1}$2$\bar{1}$] polar profiles and conversely a peak at 55° in the [1$\bar{2}$1] profiles. There is no evidence of the presence of such peaks with significant amplitudes. Moreover, it appears that the orientation of the buckled

Si top layer is opposite to that of the underlying Si(111) double layers in the substrate. In this respect, we have recorded both the surface silicide Er *MNN* Auger and the Si 2*p* core-level intensity profiles measured from a clean Si(111) substrate along a given ([$1\bar{2}1$] or [$\bar{1}2\bar{1}$]) azimuth. The relevant x-ray photoemission diffraction curves for Si 2*p* are also shown in Fig. 2. These curves are discussed in detail elsewhere.[16] Here we merely note that they can be used to identify the orientation of the substrate since they display major forward-scattering features and a rich fine-structure characteristic of a given azimuth ([$\bar{1}2\bar{1}$] or [$1\bar{2}1$]). Note for instance the skewed shape of the normal emission peak which corresponds to forward scattering from the [111] atomic row in Si and the forward-scattering peak (near 70°) from the equivalent [$11\bar{1}$] row along the [$1\bar{2}1$] azimuth. The [$1\bar{2}1$] and [$\bar{1}2\bar{1}$] azimuths referred to in the present report are determined in this way.

Finally, the $p3m1$ symmetry of the surface silicide is also reflected in our angle-resolved valence-band photoemission studies. Selected photoemission spectra using He_I photons are shown as a function of the polar angle Θ in Fig. 6 for the [$1\bar{2}1$] and [$\bar{1}2\bar{1}$] azimuths. One observes the presence of many well-resolved structures with relative intensities and binding energies varying in a drastic way with Θ. Examination of the energy dispersion along the $\bar{\Gamma}\bar{M}$ and $\bar{\Gamma}\bar{K}$ lines (not shown here) reveals 2D band dispersions $E(k_\parallel)$ consistent with a (1×1) surface periodicity.[8] In particular most structures lying in the 0–4 eV binding-energy range exhibit little or no dispersion with photon energy, having therefore a 2D origin in $k_\parallel$ space. They are either localized in the surface silicide layer as bona fide surface states or they reflect strong surface resonances. As expected, spectra taken along all the equivalent $\bar{\Gamma}\bar{K}$ directions are identical and display structures with the same energy dispersions and relative intensities. In contrast, in Fig. 6 there are striking differences between two series of spectra recorded along the two opposite [$\bar{1}2\bar{1}$] and [$1\bar{2}1$] directions. When one compares the spectra taken along the relevant $\bar{\Gamma}\bar{M}$ and $\bar{\Gamma}\bar{M}'$, azimuths at a same polar angle, one observes a marked difference in the surface state peak *intensities* whereas the relevant binding *energies* are generally identical. Occasionally, the intensity of a given peak is reduced in a drastic way along the opposite azimuth, becoming possibly hardly detectable. An example is given by the spectra at $\Theta=30°$ and 40° in the 2–4 eV binding-energy range. Some spectral peaks apparently do shift in energy with respect to the change $k_\parallel \rightarrow -k_\parallel$. This is the case for the feature observed at 20° near 3.5 eV binding energy in Fig. 6 and is due to the composite character of that peak which contains several narrow components whose relative intensities change along opposite azimuths so that an apparent shift in the center of the gravity takes place. On the other hand, Si substrate bulk band emission also contributes to the spectra and initial bulk band states probed along opposite [$1\bar{2}1$] and [$\bar{1}2\bar{1}$] azimuths are not identical for a given polar angle since they correspond to nonequivalent parts of the bulk Brillouin zone. Yet, from our large body of angle-resolved spectra, we conclude that those features with a marked 2D character and related to the surface silicide strongly change in intensity but do not shift in energy upon reversing $k_\parallel$. With the experimental geometry of Fig. 1, this implies that the [$\bar{1}2\bar{1}$] and [$1\bar{2}1$] opposite azimuths are nonequivalent for the surface silicide structure in contrast to the [$\bar{1}01$] and [$10\bar{1}$] directions. Yet, interestingly, the relevant symmetry lines in the SBZ, namely the $\bar{\Gamma}\bar{M}$ and $\bar{\Gamma}\bar{M}'$ lines and in particular the $\bar{M}$ and $\bar{M}'$ points, are found to be equivalent as far as the energy location of the surface features is concerned as expected from time-reversal symmetry which ensures $E(k_\parallel)=E(-k_\parallel)$ even if the symmetry group does not contain the inversion.

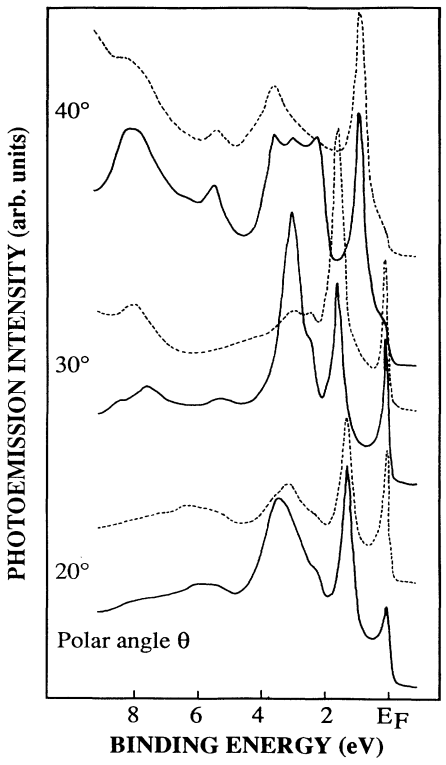

FIG. 6. Comparison between angle-resolved photoemission spectra obtained with unpolarized He_I photons for the Er surface silicide taken along the [$1\bar{2}1$] (full lines) and [$\bar{1}2\bar{1}$] (dotted lines) azimuths at emission angles of 20°, 30°, and 40°.

V. CONCLUSION

We have produced evidence that a single domain of Er silicide forms on Si(111) when one Er monolayer is annealed at 400 °C. The analysis of Auger-electron diffraction data shows that this silicide can be viewed as a single $ErSi_2$ layer (AlB_2 structure) but with a buckled Si top layer. The latter is rotated by 180° around the surface normal with respect to the similar Si double layer of the Si(111) substrate. The fact that only one domain of the surface silicide is formed is important for device applications where subsequent epitaxial Si overgrowth has to be achieved. Clearly, the monotype buckled Si top layer may provide a good template for either single domain Si re-epitaxy or merely growth of high-quality $ErSi_{1.7}$

films. The present finding of a surface silicide with a definite orientation with respect to the substrate also indicates that a specific interfacial bonding geometry of surface silicide to the substrate is energetically favored. However, no information on the interface structure can be inferred from the present data. In this respect, calculations show that data collected in the present mode (angular scans) show essentially no sensitivity to the interfacial bonding geometry. This is because scattering of the Er emission by substrate atoms involves large scattering angles. Hence, at the high kinetic energies utilized in our experiments, this implies very small scattered amplitudes.

One may invoke three different registries with respect to the Si(111) substrate, consistent with the observed 3 m point group: the Er can be located (a) in top sites, i.e., on top of Si atoms of the first Si(111) plane, (b) in T_4 sites, i.e., on top of Si atoms of the second Si(111) plane, and (c) in H_3 sites, i.e., in threefold hollow sites of the Si double layer. Since the T_4 and H_3 sites are threefold coordinated sites they most likely correspond to a lower energy than the on-top geometry. Now, it is remarkable that in these bonding configurations we get a similar bonding geometry to the Si double layer above and below the Er. These structures also most closely resemble the atomic arrangement in bulk $ErSi_2$ both above and below the hexagonal Er monolayer. As an example the T_4 geometry has been adopted in the model of Fig. 3. Among other techniques, methods exploiting backscattered amplitudes and interferences such as surface extended x-ray absorption fine-structure measurements or photoelectron holography may possibly shed some light on the interfacial bonding geometry.

ACKNOWLEDGMENT

The Laboratoire de Physique et Spectroscopie Electronique is Unité Associée au CNRS No. 1435.

[1]J. A. Knapp and S. T. Picraux, Appl. Phys. Lett. **48**, 466 (1986).

[2]F. Arnaud d'Avitaya, A. Perio, J. C. Oberlin, Y. Campidelli, and J. A. Chroboczek, Appl. Phys. Lett. **54**, 2198 (1989).

[3]F. H. Kaatz, M. P. Siegal, W. R. Graham, J. Van der Spiegel, and J. J. Santiago, Thin Solid Films **184**, 325 (1990).

[4]P. Wetzel, L. Haderbache, C. Pirri, J. C. Peruchetti, D. Bolmont, and G. Gewinner, Surf. Sci. **251/252**, 799 (1991).

[5]K. N. Tu, R. D. Thompson, and B. Y. Tsaur, Appl. Phys. Lett. **38**, 626 (1981).

[6]J. Y. Duboz, P. A. Badoz, A. Perio, J. C. Oberlin, F. Arnaud d'Avitaya, Y. Campidelli, and J. A. Chroboczek, Appl. Surf. Sci. **38**, 171 (1989).

[7]P. Paki, U. Kafader, P. Wetzel, C. Pirri, J. C. Peruchetti, D. Bolmont, and G. Gewinner, Phys. Rev. B **45**, 8490 (1992).

[8]P. Wetzel, C. Pirri, P. Paki, J. C. Peruchetti, D. Bolmont, and G. Gewinner, Solid State Commun. **82**, 235 (1992).

[9]N. W. Ashcroft and N. D. Mermin, Solid State Physics, (Saunders College Publishing, Orlando, FL, 1987).

[10]C. S. Fadley, Prog. Surf. Sci. **16**, 275 (1984).

[11]W. F. Egelhof, Jr., Crit. Rev. Solid State Mater. Sci. **16**, 213 (1990).

[12]S. Kono, S. M. Goldberg, N. F. T. Hall, and C. S. Fadley, Phys. Rev. B **22**, 6085 (1980).

[13]M. Sagurton, E. L. Bullock, R. Saiki, A. Kaduwela, C. R. Brundle, and C. S. Fadley, Phys. Rev. B **33**, 2207 (1986), and reference therein.

[14]R. Baptist, S. Ferrer, G. Grenet, and H. C. Poon, Phys. Rev. Lett. **64**, 311 (1990).

[15]L. C. Peterson, S. Kono, N. F. T. Hall, C. S. Fadley, and J. B. Pendry, Phys. Rev. Lett. **42**, 1545 (1979).

[16]P. Wetzel, C. Pirri, P. Paki, U. Kafader, D. Bolmont, and G. Gewinner (unpublished).